Molecular Cell, Vol. 15, 833–839, September 10, 2004, Copyright ©2004 by Cell Press

Three-Dimensional Structure of the Native Spliceosome by Cryo-Electron Microscopy

Short Article

Maia Azubel,[1] Sharon G. Wolf,[2] Joseph Sperling,[3] and Ruth Sperling[1,*]
[1]Department of Genetics
The Hebrew University of Jerusalem
Jerusalem 91904
Israel
[2]Department of Chemical Research Support
[3]Department of Organic Chemistry
Weizmann Institute of Science
Rehovot 76100
Israel

Summary

Splicing of pre-mRNA occurs in a multicomponent macromolecular machine—the spliceosome. The spliceosome can be assembled in vitro by a stepwise assembly of a number of snRNPs and additional proteins on exogenously added pre-mRNA. In contrast, splicing in vivo occurs in preformed particles where endogenous pre-mRNAs are packaged with all five spliceosomal U snRNPs (penta-snRNP) together with other splicing factors. Here we present a three-dimensional image reconstruction by cryo-electron microscopy of native spliceosomes, derived from cell nuclei, at a resolution of 20 Å. The structure revealed an elongated globular particle made up of two distinct subunits connected to each other leaving a tunnel in between. We show here that the larger subunit is a suitable candidate to accommodate the penta-snRNP, and that the tunnel could accommodate the pre-mRNA component of the spliceosome. The features this structure reveals provide new insight into the global architecture of the native splicing machine.

Introduction

Eukaryotic pre-mRNAs must undergo several posttranscriptional modifications before their export to the cytoplasm as functional mRNAs. Most pre-mRNAs contain intervening sequences (introns) that must be removed in order to place the coding sequences (exons) in a protein-reading frame. The mechanism of this critical processing event, known as pre-mRNA splicing, has been extensively worked out (reviewed in Brow, 2002). However, the regulation of splicing and alternative splicing, which accounts for the versatility of proteins encoded by the genome (Brett et al., 2002; Smith and Valcarcel, 2000), is still not well understood, particularly from the standpoint of the structure of the spliceosome—the macromolecular machine that catalyzes the splicing reactions.

Numerous studies in vitro have shown that the assembly of the spliceosome into a 60S ribonucleoprotein (RNP) particle occurs in a stepwise manner (Brow, 2002). This process involves an intricate series of interactions between five major uridine-rich small nuclear RNP complexes (U1, U2, U4, U5, and U6 snRNPs), as well as a number of non-snRNP splicing factors, which are dynamically recruited to the spliceosome when an exogenous pre-mRNA is added to a crude nuclear extract. Density gradient centrifugation and native gel electrophoresis revealed at least four intermediate complexes (E/CC, A, B, and C) in this assembly process. The U snRNPs are the central components of the spliceosome. They participate in splice site recognition and thus have an essential function in splicing through cooperative RNA:RNA interactions between the snRNAs and with the pre-mRNA (Brow, 2002; Staley and Guthrie, 1998).

Large RNP particles that are functional in pre-mRNA splicing and contain stoichiometric amounts of all five spliceosomal U snRNAs associated with more than 60 pre-mRNA splicing factors have been isolated from yeast nuclei (Stevens et al., 2002). This penta-snRNP complex was proposed to assemble prior to binding of the pre-mRNA substrate, thus highlighting the important role of large, preformed, complexes in pre-mRNA splicing. The apparent discrepancy between the notion of a stepwise assembly of the spliceosome in vitro, and the occurrence of a functional penta-snRNP complex in vivo, has been explained by a "holospliceosome" model in which the sequential complexes represent ordered modulations within the spliceosome (Brow, 2002). Yet, it has been pointed out that such distinct complexes, which represent intermediate states in spliceosome assembly in vitro, may not occur in vivo (Nilsen, 2002; Stevens et al., 2002).

Consistent with the notion of a preformed splicing complex, we have previously shown that freshly synthesized pre-mRNAs are packaged with all five spliceosomal U snRNPs and a number of protein splicing factors in large multicomponent nuclear RNP particles. These particles were isolated from cell nuclei and purified by density gradient centrifugation, where they sedimented as 200S complexes (Spann et al., 1989; Sperling et al., 1985). Mass measurements by scanning transmission electron microscopy (STEM) revealed that the 200S complex has a mass of 21 MDa, and that it is composed mainly of four similar subcomplexes, which are assembled together with the pre-mRNA (Müller et al., 1998). The 21 MDa complex is much larger than the 60S in vitro-assembled spliceosome, hence termed supraspliceosome. The supraspliceosome can be dissociated to subcomplexes whose mass is 4.8 MDa as determined by STEM mass measurements, which is similar to the estimated mass of the in vitro-assembled spliceosome (Müller et al., 1998). In fact, each of the individual subcomplexes resembles the 60S in vitro-assembled spliceosome also with respect to sedimentation coefficient (60S–70S), dimensions, and composition. These subcomplexes were shown to contain the five spliceosomal U snRNAs (unpublished data). Moreover, these subcomplexes are able to restore splicing activity to a micrococcal nuclease treated nuclear extract (see Supplemental Figure S1 at http://www.structure.org/cgi/content/full/

*Correspondence: sperling@vms.huji.ac.il

15/5/833/DC1). Therefore, they are referred to hereafter as native spliceosomes.

Supraspliceosomes are routinely isolated from mammalian cells, using a protocol mild enough to guarantee the preservation of the structure of native complexes present in the cell (Spann et al., 1989; Sperling et al., 1985). Three-dimensional (3D) image reconstruction of isolated supraspliceosomes by automated electron tomography of negatively stained (Sperling et al., 1997) and of frozen hydrated (Medalia et al., 2002) complexes, revealed a structure whose dimensions are 50 × 50 × 35 nm. These studies also showed that the four native spliceosomes are interconnected within the supraspliceosome in a flexible way. They may thus adopt different angular settings, and this imposes a significant restriction on reaching high resolution in EM image analysis. Therefore, for the present study we produced free individual native spliceosomes and carried out image reconstruction of frozen hydrated particles by the single-particle technique. This technique has been instrumental in the 3D image reconstruction of certain spliceosomal subcomplexes at 10 Å resolution (Golas et al., 2003; Stark et al., 2001). However, structural information at this resolution is not yet available for any of the native splicing complexes. Here we determined the 3D structure of the native spliceosome at a resolution of 20 Å. The structure reveals an elongated globular particle composed of two distinct subunits. The two subunits are interconnected to each other leaving a tunnel in between, which is a suitable candidate to accommodate the pre-mRNA.

Results

Isolation and Purification of Native Spliceosomes

To obtain free native spliceosomes, we took advantage of the high occurrence in introns of sequences that conform to the 5′ splice site consensus but are not used for splicing (Miriami et al., 2002). We have thus hybridized purified supraspliceosomes (Spann et al., 1989; Sperling and Sperling, 1998; Sperling et al., 1985) to DNA oligonucleotides of redundant sequence complementary to the consensus 5′ splice site sequence, and subjected them to RNase H digestion. The resulting complexes were purified by centrifugation in a 10%–45% glycerol gradient. Native spliceosomes sedimented at the 60S–70S region of the glycerol gradient, and aliquots from these fractions were taken for electron microscopy (EM).

To study the native spliceosomes in their natural aqueous environment, we used cryo-EM. In order to obtain the relatively high concentration of particles, which is advantageous for single-particle reconstruction, we used a positively charged lipid monolayer (Kornberg and Darst, 1991), to effectively adsorb and thus concentrate the particles while preserving their native structure (Medalia et al., 2002). A typical field of ice-embedded native spliceosomes, concentrated on a positively charged lipid monolayer, is shown in Figure 1. A 3D structure was reconstructed from 9297 raw single-particle images by first calculating an initial model using the common lines approach (Penczek et al., 1996). This initial model was then refined by using cycles of multireference alignment to reprojections of the model (see Experimental Procedures). Due to complete random orientation in the vitreous ice, representative angular views of native spliceosomes were equally populated. Figure 2 depicts a gallery of selected raw images (upper row), and the class average to which each particle was assigned (middle row), as well as the corresponding reprojections (lower row). The total number of members of each class is also indicated. After refinement, the Fourier shell correlation function (van Heel, 1987) was used to calculate the resolution of the 3D reconstruction giving values of 20 Å for the 3σ threshold criteria, and 22 Å for the 0.5 threshold criteria.

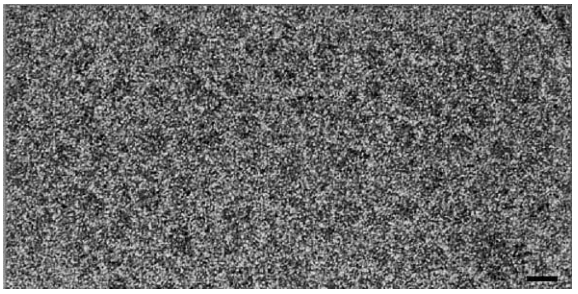

Figure 1. Native Spliceosomes

Visualization by cryo-EM of native spliceosomes. The bar represents 40 nm.

Architecture of the Native Spliceosome

The reconstructed native spliceosome presents an elongated globular structure (Figure 3), with the longest dimension (termed central axis) of 28 nm (Figure 3A). Notably, an internal division of the whole structure of the native spliceosome is visible in Figures 3D and 3F, revealing two distinct globular bodies, interconnected by a net of bridges that create the surface of interaction between these two bodies. The dimension of the larger subunit (Figure 3F, "L") along the central axis is 17 nm and the dimensions perpendicular to this axis are 24 × 22 nm. The dimensions of the smaller subunit (Figure 3F, "S") are 11 nm along the central axis and 21 × 17 nm perpendicular to this axis.

It is clear from the reconstruction that the native spliceosome has no global symmetry. Yet, it is possible to find elements that could indicate certain degree of local symmetry, such as protuberant bodies that appear similar and can be found more than once inside the particle (Figure 3E and 3F, red circles). The reconstruction also reveals that the contacts between the two subunits of the native spliceosome are achieved mostly through a group of thin necks or a net of bridges (Figure 3, green arrows). One side of the particle depicts a very compact structure (Figures 3A–3C), whereas the other side exposes a cavity inside the native spliceosome (Figures 3D–3F). In addition, several holes can be found in the interface between the two subunits. This feature is consistent with previous observation, where the presence of a hole inside the subcomplexes of the supraspliceosome was detected by cryo image restoration (see Figure 8 in Medalia et al. [2002]). Furthermore, the structure reveals a principal hole that passes through

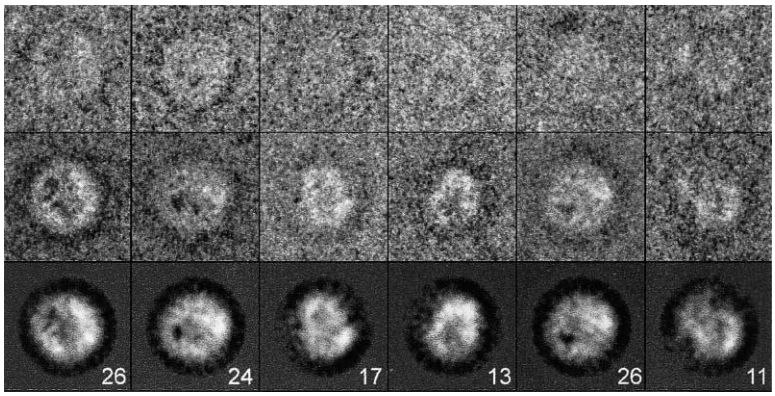

Figure 2. Single-Particle Image Reconstruction of Native Spliceosomes

A gallery of representative raw images (upper row), class averages (middle row), and corresponding reprojections (lower row). The number at the bottom of each column indicates the number of members in each represented class.

the whole particle, creating a tunnel positioned approximately in the middle of the particle (Figures 3A and 3D).

Subunit Architecture

The fact that native spliceosomes are composed of two distinct subunits was previously observed by Müller et al. (1998). In that study, the STEM images revealed a clear division inside the native spliceosome, which was observed both in the individual native spliceosome and in some orientations of the native spliceosome within the supraspliceosomal complex (see Figure 1 in Müller et al. [1998]). Consistent with this observation, the STEM mass measurements revealed two major equally populated distinct groups of small particles with masses of 1.5 and 3.1 MDa, which together add up close to the 4.8 MDa mass of the native spliceosome (Müller et al., 1998). Notably, the dimensions of each of these small particles correspond to that of the respective subunit within the native spliceosome, indicating that the native spliceosome is composed of these two distinct subunits and that the cleavage occurs at the observed division. The present 3D reconstruction of the native spliceosome corroborates this observation by showing a similar nonsymmetrical division of the particle (Figure 3F).

The two subunits are not only different in shape and size but also with respect to the distribution of high densities within the native spliceosome. Because RNA is denser than protein, the localization of regions of high density can provide some information about internal organization of RNA and protein components. Admittedly, the resolution of our reconstruction is not sufficient to assign RNA and proteins by the method described by Spahn et al. (2000). Nevertheless, it is possible to see, from the contour level representation of cross-sections of the 3D density map (Figure 4), that all the high-density regions (red lines) are placed on the large subunit. A closer examination of this density distribution reveals that the high-density regions do not

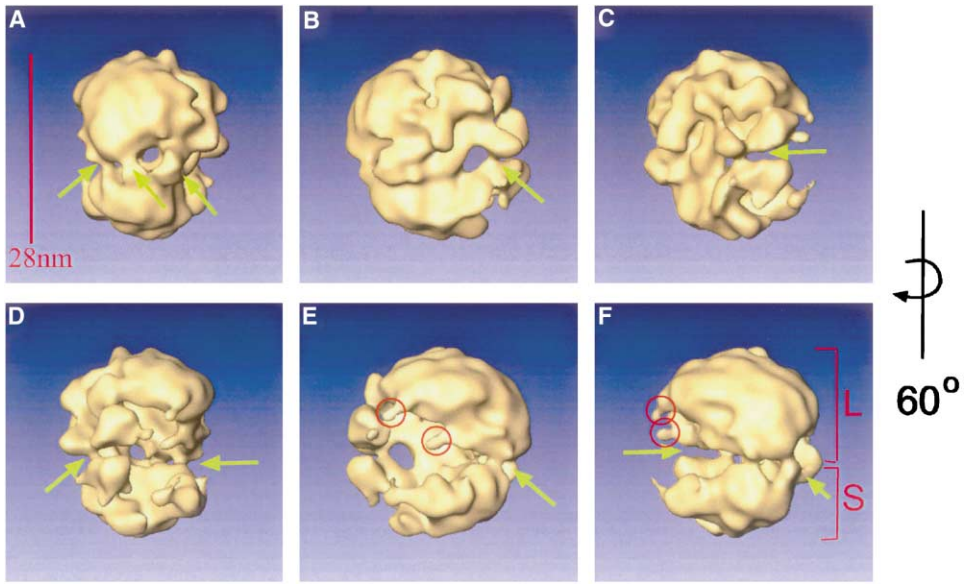

Figure 3. Surface Representation of the 3D Reconstruction of the Native Spliceosome at 20 Å Resolution

(A–F) Six views of the native spliceosome are shown, separated by rotation of 60° about the central axis. Green arrows indicate connecting points between the large (L) and small (S) subunits. Red circles indicate similar protruding bodies. The reconstruction was generated from 9297 images of unstained, frozen-hydrated particles. The threshold for rendering was chosen based on a molecular weight of 4.8 MDa for the complex (Müller et al., 1998).

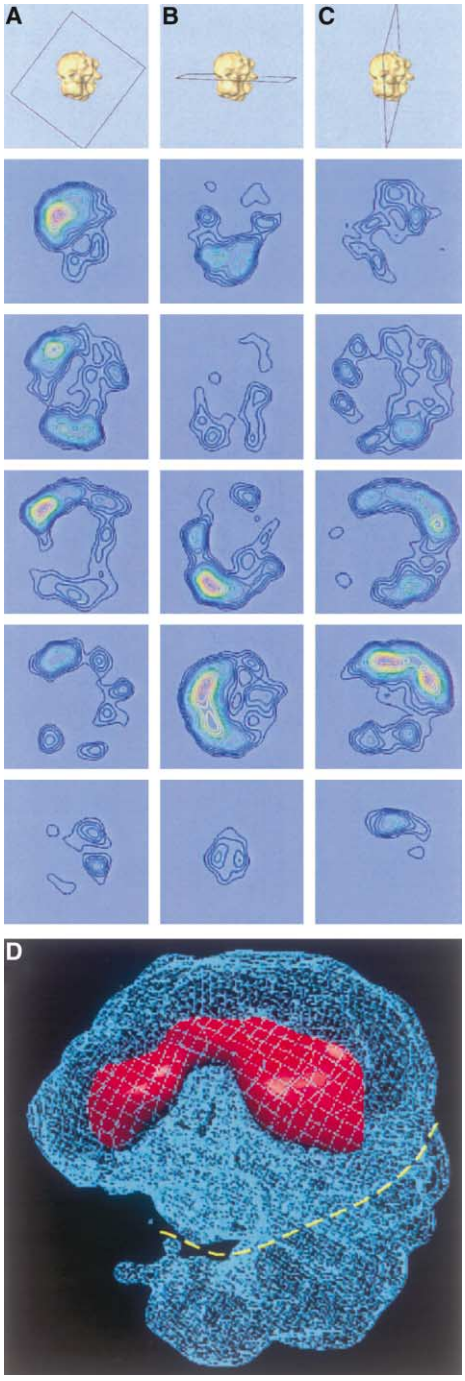

Figure 4. Density Distribution within the Native Spliceosome

(A–C) Contour level representation of cross-sections through the 3D density map of the native spliceosome. The sections, separated by 40 Å, are parallel to the planes depicted at the top of each column. (D) Surface representation of the 3D reconstruction of the native spliceosome. High-threshold rendering (red surface) shows the high-density mass region that represents the stable RNAs (see text). The division between the large and small subunits of the native spliceosome is depicted by the yellow broken line.

spread all over the large subunit. On the contrary, as visible in Figure 4A, they are placed on the left-half side of the large subunit. Figures 4B and 4C complete the picture by demonstrating that the high-density distribution is split into two regions. Figure 4D shows that they are interconnected, which is in good agreement with the fact that the spliceosomal U snRNAs are involved in several base-pairing interactions with each other to make the spliceosome functional (Brow, 2002). Moreover, it can be estimated that the U snRNAs occupy 4% of the total volume of the native spliceosome. Accordingly, Figure 4D shows that high-threshold rendering (red surface) that encloses the densest 4% of the total volume is entirely located within the large subunit of the native spliceosome. Thus, the high-density distribution suggests an internal organization where all the stable RNA components—the five spliceosomal U snRNAs—of the native spliceosome are placed in the large subunit.

Discussion

Bridges, a Cavity, and a Tunnel in Native Spliceosomes

This study presents the 3D structure of the native spliceosome at a resolution of 20 Å, which is the highest resolution available to date for spliceosomes derived from living cells in an intact form. The structure reveals new features of the native spliceosome, including a cavity, a tunnel, and bridges that connect between two distinct subunits.

The cavity inside the native spliceosome could provide a place to transiently store the pre-mRNA. As the number of bases that are involved in the splicing reaction represents only a small fraction of the entire labile pre-mRNA, the cavity might protect the part that is not directly involved in the splicing reaction from nonspecific degradation. The net of bridges provides a way by which the two subunits can interact at different places and, at the same time, keep the actual contact interaction to a minimum. This dual characteristic may confer stability to the whole particle and also may allow a certain degree of elasticity between the two subunits. In that case, it is possible to propose a model in which, under certain circumstances, the cavity closes up providing differential protection to the pre-mRNA to allow its continual processing.

The structure of the native spliceosome is made up of two distinct subunits connected to each other, leaving a tunnel in between. The diameter of this tunnel is variable, but at the narrowest region it reaches 15 Å, which is large enough for the RNA in an extended conformation (Robertus et al., 1974) to pass through (Hewat and Blaas, 2004). Tunnels or channels have been shown to characterize macromolecular machines involved in the metabolism of biopolymers (e.g., ribosomes in protein synthesis [Berisio et al., 2003] and RNA polymerase II in transcription [Bushnell et al., 2002]), providing a transport route for the biopolymer while it is being processed. By analogy, the tunnel observed here is a suitable candidate to accommodate the pre-mRNA component of the native spliceosome.

The Large Subunit of the Native Spliceosome Is a Suitable Candidate to Accommodate the Penta-snRNP

U1 snRNP is the smallest of the spliceosomal U snRNPs, having a mass of ~0.24 MDa (Stark et al., 2001). The

mass of the other spliceosomal U snRNPs has not been measured but can be estimated either based on their sedimentation coefficient (Müller et al., 1998) or by taking into account the biochemical information of their major components. From several proteomics studies (Gottschalk et al., 1999; Rappsilber et al., 2002; Stevens et al., 2002; Will et al., 2002) the averaged estimated mass of U2 snRNP is 1.3 MDa, and the averaged estimated mass of the U4/U6.U5 tri-snRNP is 1.5 MDa. Altogether, the estimated mass of the five spliceosomal U snRNPs is about 3.0 MDa, which is close to the 3.1 MDa mass of the large subunit of the native spliceosome as determined by STEM (Müller et al., 1998). Thus, it is reasonable to propose a model in which the large subunit of the native spliceosome harbors the penta-snRNP. This model is supported by the distribution of high densities within the reconstructed native spliceosome (Figure 4). Since RNA is denser than proteins, the stable RNA components of the native spliceosome have been assigned here to the high-density regions. This assignment, which places the spliceosomal U snRNAs in close proximity, is also consistent with previous studies that have shown multiple base pairing interactions among the spliceosomal U snRNPs (reviewed in Staley and Guthrie, 1998).

In addition, the volume of the spliceosomal U snRNPs, as estimated from the available structural information, is similar to the measured volume of the large subunit, thereby reinforcing the model. Specifically, based on the 3D model of U1 snRNP (Stark et al., 2001), U2 snRNP, and U4/U6.U5 tri-snRNP 2D images (Kastner, 1998), together with their estimated masses (see above), the estimated volume of the penta snRNP is 4300 nm^3, whereas the volume of the large subunit of the native spliceosome is 4200 nm^3.

Although alternative internal organizations are possible, the one presented here is consistent with all the biochemical and structural data currently available. These include the mass calculation, the volume estimation, and stable RNA localization by observation of high-density distribution. All these observations are consistent with the model in which the large subunit of the native spliceosome is assigned as the penta-snRNP. The non-snRNP splicing factors may then be assigned to the small subunit. Direct localization studies are required to confirm this proposal. Nonetheless, the proposed assignment of the five spliceosomal U snRNPs to the large subunit is further supported by the identification of the penta-snRNP complex from yeast (Stevens et al., 2002). This complex was shown to assemble prior to binding of the pre-mRNA substrate and to act as a functional module. The occurrence of the preassembled penta-snRNP is consistent with the supraspliceosomal model (discussed below), in the sense that the assembly of the splicing machine with the intron is brought about by simultaneous multiple interactions, rather than by a stepwise assembly of spliceosomes as inferred from earlier studies in vitro.

The Native Spliceosome: The Building Block of the Supraspliceosome

Studies of splicing in vitro brought about the concept that spliceosomes are assembled in a stepwise manner (Brow, 2002). In this context, it should be pointed out that while this work was written up, 3D reconstructions of two intermediates of the in vitro-assembled spliceosome were published: the C complex spliceosome, which contains three of the five spliceosomal U snRNAs at 30 Å resolution (Jurica et al., 2004), and a precatalytic spliceosomal complex B lacking U1 snRNP, at 40 Å resolution (Boehringer et al., 2004). From a biological point of view, a comparison between these complexes and the native spliceosome is difficult to make because it has not been established that these intermediate complexes occur in vivo (Nilsen, 2002; Stevens et al., 2002). Nevertheless, it is interesting to note that the dimensions of these complexes appear to be similar to those of the native spliceosome.

The 3D reconstruction of the native spliceosome presents a structure that is not only consistent with previous structural and biochemical data but also brings new architectural insight that helps understand the splicing phenomenon. The supraspliceosome represents a standalone complete macromolecular machine capable of performing splicing of every pre-mRNA independent of its length or number of introns (Spann et al., 1989). Within the supraspliceosome, the pre-mRNA can be processed simultaneously at four sites, as each native spliceosome is capable of processing one intron at a time. The cavity inside the native spliceosome may represent a transient storage place for pre-mRNA sequences that are not directly involved in the ongoing splicing reaction. The tunnel inside the native spliceosome may provide a passage through which the pre-mRNA and other splicing factors could pass through. In that way, efficient communication between the subcomplexes of the supraspliceosome is guaranteed, in order to correctly identify splice sites and ensure the ligation of exons in the correct manner. Such an accurate and efficient communication is important to allow the nonsequential removal of introns (Kessler et al., 1993), and is essential for splicing regulation and alternative splicing (for a comprehensive discussion see Müller et al. [1998] and Sperling et al. [1997]).

The assembly of the splicing machine with the pre-mRNA in vivo is probably brought about by simultaneous multiple interactions, rather than by a stepwise manner as inferred from studies in vitro. Such a large number of interactions that the cell has to deal with can be regulated within the supraspliceosome. Having the native spliceosomes as the building blocks of this large macromolecular assembly, this large number of interactions can be compartmentalized into each intron that is being processed. At the same time, the whole supraspliceosome enables the communication between the native spliceosomes, which is needed for regulated splicing. The organization of the supraspliceosome, like other macromolecular assemblies that exist as preformed entities, avoids the necessity to recruit the multitude of splicing components each time the spliceosome turns over. In that sense, the overall coordination of the cellular interactions is reduced from the hard work of repeatedly placing each piece in the correct position of the puzzle to the relatively simpler work of coordinating the preformed puzzle.

Experimental Procedures

Isolation of Purified Native Spliceosomes

Purified supraspliceosomes (Spann et al., 1989; Sperling and Sperling, 1998; Sperling et al., 1985), prepared from HeLa cell nuclei (CILBIOTECH, Mons, Belgium), were incubated with DNA-oligonucleotides of redundant sequence complementary to the 5′ splice site consensus sequence (AGGTRAGT) and subjected to RNase H digestion. The treated sample was centrifuged in a second 10%–45% glycerol gradient, and the native spliceosomes were collected in aliquots from fractions corresponding to the 60S–70S region of the gradient.

Cryo-EM

For cryo-EM, native spliceosomes were incubated for 20 min on a charged lipid monolayer, sampled on a grid coated with holey carbon film, and washed with water as described (Medalia et al., 2002). The frozen-hydrated samples were imaged under low-dose conditions ($\leq 10\ e^{-}/Å^{2}$) at a magnification of 93,620 and at a defocus range from -1.0 to $-4.0\ \mu m$, using an FEI (Eindhoven, The Netherlands) Tecnai F20 FEG transmission electron microscope (TEM) operating at 200 KV and equipped with a 1 k $\times$ 1 k TEMcam CCD camera (pixel size 24 μm) (TVIPS, Gauting, Germany), with an effective sampling of 0.26 nm/pixel in the images.

Single-Particle Image Reconstruction

The Boxer procedure from the EMAN software package (Ludtke et al., 1999) was used to collect 9297 single-particle images. The 3D reconstruction using this data set was performed with the SPIDER software package (Frank et al., 1996). Low-pass filtered single-particle images were subjected to a reference-free alignment procedure and hierarchical classification. The class averages were then computed and an initial 3D model was obtained using the common-lines technique (Penczek et al., 1996). The robustness of this procedure is demonstrated in Supplemental Table S1 and Figure S2. Refinement of the structure was performed after contrast-transfer phase-flip correction of the raw single-particle images (done with the CTFIT procedure of the EMAN software package [Ludtke et al., 1999]), using the back-projected images from the initial model in a multireference alignment and classification procedure. For each refinement cycle, the particle images with the lowest 20% crosscorrelation coefficient were excluded from the reconstruction. The removed particles were reconsidered in the next iteration, and 89% of the rejected particles were consistently rejected in the subsequent cycles. The Fourier shell correlation function (van Heel, 1987) was used to calculate the resolution of the 3D reconstruction with values of 20 Å for the 3σ threshold criteria and 22 Å for the 0.5 threshold criteria. The Amira software package was used for the surface rendering of the reconstruction.

Acknowledgments

We thank Aaron Klug, Ada Yonath, Roger Kornberg, and Andreas Engel for critically reading the manuscript and for helpful suggestions.

We thank Mrs. Aviva Pecho for technical assistance. This research was funded by grants from the Israel-US Binational Science Foundation (R.S.) and the Helen and Milton Kimmelman Center for Biomolecular Structure and Assembly at the Weizmann Institute of Science (J.S.).

Received: April 1, 2004
Revised: June 24, 2004
Accepted: June 29, 2004
Published: September 9, 2004

References

Berisio, R., Schluenzen, F., Harms, J., Bashan, A., Auerbach, T., Baram, D., and Yonath, A. (2003). Structural insight into the role of the ribosomal tunnel in cellular regulation. Nat. Struct. Biol. *10*, 366–370.

Boehringer, D., Makarov, E.M., Sander, B., Makarova, O.V., Kastner, B., Lührmann, R., and Stark, H. (2004). Three-dimensional structure of a pre-catalytic human spliceosomal complex B. Nat. Struct. Mol. Biol. *11*, 463–468.

Brett, D., Pospisil, H., Valcárcel, J., Reich, J., and Bork, P. (2002). Alternative splicing and genome complexity. Nat. Genet. *30*, 29–30.

Brow, D.A. (2002). Allosteric cascade of spliceosome activation. Annu. Rev. Genet. *36*, 333–360.

Bushnell, D.A., Cramer, P., and Kornberg, R.D. (2002). Structural basis of transcription: alpha-amanitin-RNA polymerase II cocrystal at 2.8 Å resolution. Proc. Natl. Acad. Sci. USA *99*, 1218–1222.

Frank, J., Radermacher, M., Penczek, P., Zhu, J., Li, Y., Ladjadj, M., and Leith, A. (1996). SPIDER and WEB: processing and visualization of images in 3D electron microscopy and related fields. J. Struct. Biol. *116*, 190–199.

Golas, M.M., Sander, B., Will, C.L., Lührmann, R., and Stark, H. (2003). Molecular architecture of the multiprotein splicing factor SF3b. Science *300*, 980–984.

Gottschalk, A., Neubauer, G., Banroques, J., Mann, M., Lührmann, R., and Fabrizio, P. (1999). Identification by mass spectrometry and functional analysis of novel proteins of the yeast [U4/U6.U5] tri-snRNP. EMBO J. *18*, 4535–4548.

Hewat, E.A., and Blaas, D. (2004). Cryoelectron microscopy analysis of the structural changes associated with human rhinovirus type 14 uncoating. J. Virol. *78*, 2935–2942.

Jurica, M.S., Sousa, D., Moore, M.J., and Grigorieff, N. (2004). Three-dimensional structure of C complex spliceosomes by electron microscopy. Nat. Struct. Mol. Biol. *11*, 265–269.

Kastner, B. (1998). Purification and electron microscopy of spliceosomal snRNPs. In RNP Particles, Splicing and Autoimmune Diseases, J. Schenkel, ed. (Berlin: Springer), pp. 95–140.

Kessler, O., Jiang, Y., and Chasin, L.A. (1993). Order of intron removal during splicing of endogenous adenine phosphoribosyltransferase and dihydrofolate reductase pre-mRNA. Mol. Cell. Biol. *13*, 6211–6222.

Kornberg, R.D., and Darst, S.A. (1991). Two-dimensional crystals of proteins on lipid layers. Curr. Opin. Struct. Biol. *1*, 642–646.

Ludtke, S.J., Baldwin, P.R., and Chiu, W. (1999). EMAN: semiautomated software for high-resolution single-particle reconstructions. J. Struct. Biol. *128*, 82–97.

Medalia, O., Typke, D., Hegerl, R., Angenitzki, M., Sperling, J., and Sperling, R. (2002). Cryoelectron microscopy and cryoelectron tomography of the nuclear pre-mRNA processing machine. J. Struct. Biol. *138*, 74–84.

Miriami, E., Motro, U., Sperling, J., and Sperling, R. (2002). Conservation of an open-reading frame as an element affecting 5′ splice site selection. J. Struct. Biol. *140*, 116–122.

Müller, S., Wolpensinger, B., Angenitzki, M., Engel, A., Sperling, J., and Sperling, R. (1998). A supraspliceosome model for large nuclear ribonucleoprotein particles based on mass determinations by scanning transmission electron microscopy. J. Mol. Biol. *283*, 383–394.

Nilsen, T.W. (2002). The spliceosome: no assembly required? Mol. Cell *9*, 8–9.

Penczek, P.A., Zhu, J., and Frank, J. (1996). A common-lines based method for determining orientations for $N > 3$ particle projections simultaneously. Ultramicroscopy *63*, 205–218.

Rappsilber, J., Ryder, U., Lamond, A.I., and Mann, M. (2002). Large-scale proteomic analysis of the human spliceosome. Genome Res. *12*, 1231–1245.

Robertus, J.D., Ladner, J.E., Finch, J.T., Rhodes, D., Brown, R.S., Clark, B.F., and Klug, A. (1974). Structure of yeast phenylalanine tRNA at 3 Å resolution. Nature *250*, 546–551.

Smith, C.W., and Valcárcel, J. (2000). Alternative pre-mRNA splicing: the logic of combinatorial control. Trends Biochem. Sci. *25*, 381–388.

Spahn, C.M., Penczek, P.A., Leith, A., and Frank, J. (2000). A method for differentiating proteins from nucleic acids in intermediate-resolution density maps: cryo-electron microscopy defines the quaternary structure of the Escherichia coli 70S ribosome. Struct. Fold. Des. *8*, 937–948.

Spann, P., Feinerman, M., Sperling, J., and Sperling, R. (1989). Isolation and visualization of large compact ribonucleoprotein particles of specific nuclear RNAs. Proc. Natl. Acad. Sci. USA *86*, 466–470.

Sperling, R., and Sperling, J. (1998). The lnRNP particle: a naturally assembled complex of pre-mRNA and splicing factors. In RNP Particles, Splicing and Autoimmune Diseases, J. Schenkel, ed. (Berlin: Springer), pp. 29–47.

Sperling, R., Sperling, J., Levine, A.D., Spann, P., Stark, G.R., and Kornberg, R.D. (1985). Abundant nuclear ribonucleoprotein form of CAD RNA. Mol. Cell. Biol. *5*, 569–575.

Sperling, R., Koster, A.J., Melamed-Bessudo, C., Rubinstein, A., Angenitzki, M., Berkovitch-Yellin, Z., and Sperling, J. (1997). Three-dimensional image reconstruction of large nuclear RNP (lnRNP) particles by automated electron tomography. J. Mol. Biol. *267*, 570–583.

Staley, J.P., and Guthrie, C. (1998). Mechanical devices of the spliceosome: motors, clocks, springs, and things. Cell *92*, 315–326.

Stark, H., Dube, P., Lührmann, R., and Kastner, B. (2001). Arrangement of RNA and proteins in the spliceosomal U1 small nuclear ribonucleoprotein particle. Nature *409*, 539–542.

Stevens, S.W., Ryan, D.E., Ge, H.Y., Moore, R.E., Young, M.K., Lee, T.D., and Abelson, J. (2002). Composition and functional characterization of the yeast spliceosomal penta-snRNP. Mol. Cell *9*, 31–44.

van Heel, M. (1987). Similarity measures between images. Ultramicroscopy *21*, 95–100.

Will, C.L., Urlaub, H., Achsel, T., Gentzel, M., Wilm, M., and Lührmann, R. (2002). Characterization of novel SF3b and 17S U2 snRNP proteins, including a human Prp5p homologue and an SF3b DEAD-box protein. EMBO J. *21*, 4978–4988.